Topological edge states in a Rydberg composite

Matthew T. Eiles [1,*] Christopher W. Wächtler [1,2] Alexander Eisfeld [1,3] and Jan M. Rost [1]

[1] *Max-Planck-Institut für Physik komplexer Systeme, Nöthnitzer Str. 38, D-01187 Dresden, Germany*

[2] *Department of Physics, University of California, Berkeley, California 94720, USA*

[3] *Universität Potsdam, Institut für Physik und Astronomie, Karl-Liebknecht-Str. 24-25, 14476 Potsdam, Germany*

(Received 6 September 2023; revised 13 December 2023; accepted 26 January 2024; published 20 February 2024)

We examine topological phases and symmetry-protected electronic edge states in the context of a Rydberg composite: a Rydberg atom interfaced with a structured arrangement of ground-state atoms. We show that the spectrum of the electronic Hamiltonian of such a composite possesses a mapping to that of a tight-binding Hamiltonian, which can exhibit nontrivial topology depending on the arrangement of the ground-state atoms and the principal quantum number of the Rydberg state. The Rydberg electron moves in a combined potential including the long-ranged Coulomb interaction with the Rydberg core and short-ranged interactions with each neutral atom; the effective hopping amplitudes between sites are determined by this combination. We first confirm the existence of topologically-protected edge states in a Rydberg composite by mapping it to the paradigmatic Su-Schrieffer-Heeger dimer model. Following that, we show that more complicated systems with trimer unit cells can be studied in a Rydberg composite.

DOI: 10.1103/PhysRevB.109.075422

I. INTRODUCTION

Topological insulators [1–3] describe a special class of solids exhibiting an insulating bulk but conducting surface states. These display a surprising immunity to a wide range of local deformations, inherently avoiding backscattering over broad energy ranges and circumventing localization in the presence of disorder. Questions about the existence, behavior, and characterization of topological insulators and the symmetry-protected edge states that they can host have motivated rapid growth in this field in recent years [4–22]. A major effort in this direction is the exploration of well-controlled systems that exhibit novel topological properties and can be used to clarify questions about the behavior of topological invariants. Ultracold Rydberg atoms are promising quantum simulators in this respect due to their high controllability and exaggerated properties. Two recent examples using very different approaches illustrate this in the context of the Su-Schrieffer-Heeger (SSH) model [23]. In the first, several Rydberg atoms were arranged in an optical tweezer array. The long-range dipolar interactions between two Rydberg states of different angular momentum enabled the desired staggered hopping amplitudes [24]. In the second example, multiple Rydberg levels of a single atom were employed to form a synthetic one-dimensional lattice, with microwave coupling between these levels setting the hopping amplitudes [25]. The design of simulators of topologically richer systems than the SSH model remains an area of active research, with most proposals utilizing the long-range interactions between Rydberg atoms prepared in complicated geometries [26–32]. As experimental progress towards fully programmable optical tweezer arrays accelerates, these proposals become approachable.

Alongside the simulation of topological systems, it is also of fundamental interest to study how the topological concepts established in solid-state theory can emerge in other types of systems. Motivated by this, in the present article we consider a topologically nontrivial Rydberg system that is conceptually different from the ones mentioned above, namely a *single* Rydberg atom and an ensemble of ground-state atoms (scatterers) located within the Rydberg electron's orbit. Confinement of these scatterers in a particular arrangement could be provided by an optical lattice or an array of optical tweezers. Such a *Rydberg composite* allows for the design of Hamiltonians which exhibit features associated with symmetry-protected topological insulators. The topological properties exhibited by the Rydberg electron can be tuned by the choice of the scatterer positions and by the principal quantum number ν, and are manifest in the spatial structure of the electronic wavefunction and in the spectral density of the Rydberg atom. To demonstrate this, we consider three different topologically interesting models of increasing complexity.

II. SYSTEM HAMILTONIAN

The Hamiltonian of a Rydberg composite, with scatterers placed at positions $\vec{R}_q$, is

$$H_e = -\frac{\nabla^2}{2} - \frac{1}{r} + \sum_{q=1}^{M} 2\pi a_s \delta^3(\vec{r} - \vec{R}_q) \tag{1}$$

in atomic units [33–36]. The first two terms govern the electron's motion in the Coulomb field of the Rydberg core, while

*meiles@pks.mpg.de

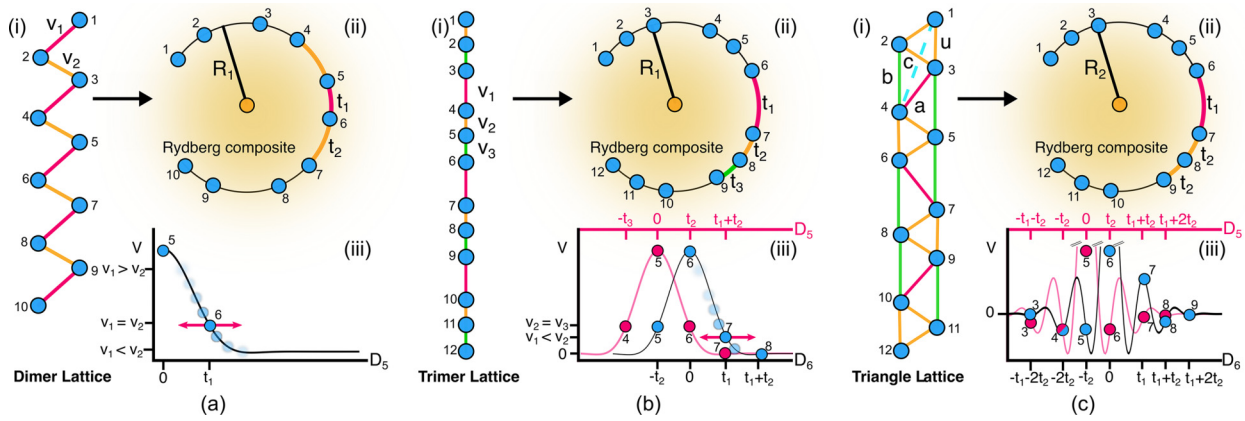

FIG. 1. Schematics of the three models: (a) dimer SSH chain, (b) trimer SSH chain, and (c) triangle chain. In each panel, (i) depicts the desired tight-binding lattice and defines the couplings between sites, and (ii) sketches the Rydberg composite corresponding to this lattice. The arc lengths shown in this panel determine the effective couplings, as illustrated in each panel by (iii), which shows the relevant interaction curves. The interaction curve V in (a iii) shows the hopping amplitude between site 5 and neighboring sites as a function of D_5, the distance around the circle away from site 5. As the position of site 6 moves, so does the energy V_{56} (blue circle marked 6), modifying the ratio v_2/v_1. Two different interaction curves are shown in (b iii). The black (pink) curve shows the interaction V as a function of the distance D_6 (D_5) away from site 6 (5). The blue markers denote the onsite potential E_6 and hopping amplitudes V_{65}, V_{67}, and V_{68}; the pink markers show E_5, V_{54}, V_{56}, and V_{57}. The next-nearest-neighbor amplitudes V_{68} and V_{57} are negligible. By varying t_1, the distance between sites 6 and 7 is changed, which modifies V_{67} while keeping constant the other interactions. Panel (c iii) shows these same interaction curves, but now in the more complicated geometry relevant to the triangle lattice. Careful inspection of the different points on these two curves shows how the hopping amplitudes u, a, b, and c in the triangle lattice are realized; the amplitude u is fixed for this geometry, while the other amplitudes vary as a function of t_1.

the last term describes its interaction with the scatterers using the Fermi pseudopotential, valid in the low-energy scattering limit. The interaction strength is determined by the s-wave scattering length a_s [37,38], and is is too weak to mix Rydberg states with different principal quantum numbers ν [39,40]. Instead, it splits the degenerate Rydberg levels with different angular momentum l but the same ν into two subspaces [41]. The first, of size $\nu^2 - M$, remains degenerate and unshifted, while the second, of size M, splits away [34,38]. It is in this shifted manifold that topologically protected edge states can be realized.

It is convenient to transform the Hamiltonian Eq. (1) to have the structure of a tight-binding Hamiltonian so that it is clear how to tune the parameters of the Rydberg system—the scatterer positions and principal quantum number—to realize desired hopping terms or onsite potentials for a given topologically interesting system. We recently derived such a transformation in Ref. [34], and do not present the full details here. In short, the transformation utilizes the fact that the matrix representation of H_e within a degenerate Rydberg manifold can be written $H_e = \mathcal{W}\mathcal{W}^\dagger$. $\mathcal{W}$ is a rectangular matrix of dimension $\nu^2 \times M$ with matrix elements $\sqrt{2\pi a_s}\phi^*_{nlm}(\vec{R}_q)$, where $\phi_{\nu lm}(\vec{r}) = \frac{u_{\nu l}(r)}{r} Y_{lm}(\hat{r})$ is a hydrogenic wave function. Reminiscent of the construction of pair Hamiltonians in the formulation of supersymmetric quantum mechanics [42], the spectrum of this Hamiltonian, except for its zero-energy states, is identical to that of the Hamiltonian $H = \mathcal{W}^\dagger\mathcal{W}$. H is an $M \times M$ matrix with the form

$$H = \sum_q^M E_q |q\rangle\langle q| + \sum_q^M \sum_{q' \neq q}^M V_{qq'} |q\rangle\langle q'|. \tag{2}$$

The state $|q\rangle$ describes a wavefunction which is localized on the scatterer at position $\vec{R}_q$. Since the spectrum of this Hamiltonian coincides *exactly*, within the stated approximations, with that of the Hamiltonian H_e it is possible to realize a given H by tuning the parameters of H_e to achieve the desired matrix elements E_q and $V_{qq'}$. In the high ν limit where the effect of quantum-defect-shifted states is negligible, these matrix elements are given in closed form [38]:

$$V_{qq'} = 2\pi a_s \frac{u'_{\nu 0}(x_-)u_{\nu 0}(x_+) - u_{\nu 0}(t_-)u'_{\nu 0}(x_+)}{2(x_+ - x_-)}. \tag{3}$$

Here, $x_\pm = \frac{1}{2}(R_q + R_{q'} \pm |\vec{R}_q - \vec{R}_{q'}|)$, $R_q = |\vec{R}_q|$, and $u_{\nu 0}(r)$ is the s-wave reduced-hydrogen radial function. The prime denotes the spatial derivative.

III. REALIZATION OF TOPOLOGICAL MODELS

The three composites illustrated in Fig. 1 exemplify the ability of different scatterer arrangements, in combination with the choice of Rydberg state ν, to realize different effective lattice Hamiltonians. We will use these three composites to demonstrate topological physics in a Rydberg composite. In each case, we consider atoms arranged in a (broken) ring around the Rydberg atom, which fixes a common E_q for all scatterers. We select the number of scatterers M, the principal quantum number ν, and radius $R = R_q$ such that the desired hopping terms $V_{qq'}$ are realized. To confirm that this leads to a topologically nontrivial configuration, we theoretically analyze each setup by applying periodic boundary conditions to the effective Hamiltonian, giving insight into its topological bulk properties. The bulk-boundary correspondence allows us to subsequently ascertain its topological aspects in the finite system.

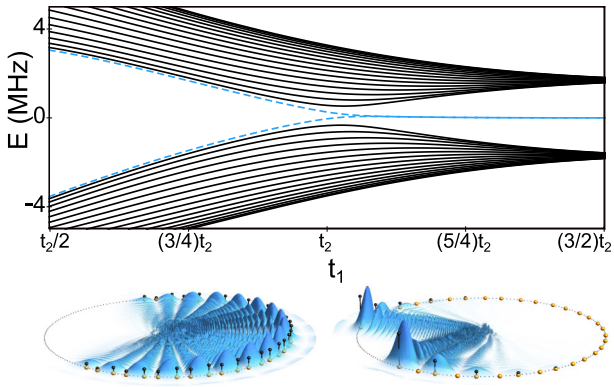

FIG. 2. The energy spectrum of the dimer SSH Rydberg composite, where $\nu = 60$ and $R = 2\nu^2$. The energies are centered around the onsite potential E_q, and are plotted as a function of t_1 for fixed $t_2 = 2\pi R/45$. The exemplary wavefunction images shown below the spectrum illustrate the bulk eigenstate corresponding to the dashed-blue level in the upper band (left, $t_1 = 3t_2/4$) and an edge state (right, $t_1 = 5t_2/4$).

A. SSH model (dimer lattice)

The first model that we consider is the dimer SSH model depicted in Fig. 1(ai): a one-dimensional lattice with staggered nearest-neighbor hopping amplitudes v_1 and v_2 [23]. This paradigmatic model introduces many concepts useful in the analysis of more complicated systems. Fig. 1(aii) shows how to design a Rydberg composite which realizes this model. We set $R = R_1 = 2\nu^2$ and place the scatterers on this ring so that they are separated by arclengths t_1 and t_2. By choosing $M < \nu$ we guarantee that the scatterers are spaced sufficiently far apart so that $V_{qq'}$ is negligible when $|q' - q| > 1$ [34]. Then, the monotonic dependence of $V_{qq'}$ on t_1 allows us to stagger the hopping elements simply by staggering the distances t_1 and t_2, as is illustrated in Fig. 1(aiii). For illustrative purposes we choose $\nu = 60$, $M = 36$, and fix $t_2 = 2\pi R/45$. These choices yield a reasonably large number of lattice sites without making the resulting band spectrum and wavefunctions overly complicated to visualize. The spacing between atoms in this configuration, around 50 nm, is at the leading edge of current experimental capabilities for trapping nearby atoms [43,44]. Figure 2 shows the resulting eigenspectrum as a function of t_1. It consists of two distinct bands separated by an empty band gap when $t_2 > t_1$, i.e., when $v_1 > v_2$ [see Fig. 1(ai)]. This band gap closes when $t_1 = t_2$. When $t_1 > t_2$, the hopping amplitudes satisfy $v_2 > v_1$ and the two levels closest to the band gap, highlighted in blue, split from the bulk and become degenerate at the center of the spectrum. Investigation of the eigenstates of these levels shows that they evolve from bulk states spread over the entire composite when $t_2 < t_1$ to edge states appearing at the boundary of the chain of scatterers when $t_1 > t_2$. In the two eigenstates depicted in Fig. 2, the black spheres represent the wavefunction in the site basis used to describe H in Eq. (2), while the blue wavefunction shows the full electronic wavefunction in position space [45].

The existence of this transition from bulk states living in the energy bands to edge states situated at the center of the band gap can be understood after considering the bulk momentum Hamiltonian

$$H_{\mathrm{SSH}}(k) = \begin{pmatrix} 0 & v_1 + v_2 e^{-ik} \\ v_1 + v_2 e^{ik} & 0 \end{pmatrix}, \tag{4}$$

which is obtained by applying periodic boundary conditions to the lattice in Fig. 1(ai). For the one-dimensional systems studied here, the Zak phase

$$\mathcal{Z} = i \int_{-\pi}^{\pi} \langle \psi_k | \partial_k \psi_k \rangle dk, \tag{5}$$

where $|\psi_k\rangle$ is an eigenstate of $H(k)$, is a quantized topological invariant which can only take the values zero or π (modulo 2π) as long as a symmetry is present [46]. The chiral symmetry of the SSH model ensures that such a topological invariant exists. Computation of the Zak phase using the eigenstates of Eq. (4) gives $\mathcal{Z} = \pi$ when $t_2 > t_1$ and $\mathcal{Z} = 0$ when $t_2 < t_1$ [47–49].

The Zak phase is intimately related to the existence of edge states through the bulk-boundary correspondence: the change in the Zak phase at $t_1 = t_2$ reveals a topological phase transition and the appearance of edge states in the finite-sized system [23,46]. The implications of these edge states are manifold. If the scatterers are not perfectly positioned at their angles on the ring, the hopping amplitudes $V_{qq'}$ become disordered but the chiral symmetry of the lattice is preserved. In such a case, although states in the bands will become localized due to this disorder, these edge states will remain unperturbed due to the symmetry protection afforded by the topology of the system. In contrast, disorder of the atom positions in the radial direction leads to diagonal disorder and a breakdown of the chiral symmetry. Consequently, the edge states are no longer symmetry protected and become indistinguishable from the band. Moving beyond the SSH model or random disorder, one could modify the onsite potentials in a controlled fashion by shifting the scatterers to slightly different ring radii, therefore simulating the Rice-Mele model [50].

B. SSH model (trimer lattice)

The second model we consider is a variation on the SSH model where the dimer unit cells are replaced with trimers. This model, shown in Fig. 1(bi), was very recently explored theoretically [51,52] as well as experimentally [53–55]. The sites within each trimer unit cell are coupled by v_2 and v_3, and the trimers are coupled via v_1. We realize this model in our composite setup by keeping the Rydberg parameters as before, which guarantees nearest-neighbor hopping, but now placing the scatterers in a different geometry, as seen in Fig. 1(bii). Applying periodic boundary conditions to the resulting Hamiltonian yields the bulk momentum Hamiltonian

$$H_{\mathrm{trimer}}(k) = \begin{pmatrix} 0 & v_2 & v_1 e^{-ik} \\ v_2 & 0 & v_3 \\ v_1 e^{ik} & v_3 & 0 \end{pmatrix}. \tag{6}$$

The topological nature of this model stems from an inversion symmetry when $v_2 = v_3$. When $v_1 = v_2 = v_3$, i.e., in the absence of trimerization, a phase transition occurs. In the Rydberg composite setting, we ensure the inversion symmetry by setting $t_2 = t_3$. By varying t_1 to change v_1 we sweep the

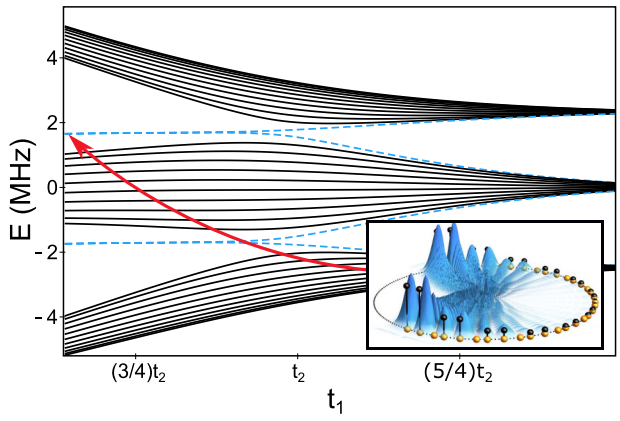

FIG. 3. The energy spectrum of the trimer SSH Rydberg composite, where $\nu = 60$ and $R = 2\nu^2$. The energies are centered around the onsite potential E_q, and are plotted as a function of t_1 for fixed $t_2 = t_3 = 2\pi R/45$. One of the edge states is shown in the inset.

system through the topological phase transition, as can be seen in the energy spectrum shown in Fig. 3. The lower band is characterized by a Zak phase $\mathcal{Z} = \pi$ when $v_1 > v_2, v_3$ which implies the existence of a pair of topologically protected edge states in the lower band gap. In the Rydberg composite, this energy relationship is satisfied when the distance t_1 is smaller than t_2 and t_3, and we see in Fig. 3 that edge states appear as expected. The Zak phase of the middle band is zero for all v_1, and since the existence of edge modes in the upper band gap is connected to the sum of the Zak phases of all bands below it, localized boundary modes must also exist in the upper band gap. One of the edge states is shown in the inset of Fig. 3. The more complicated case of a noninversion symmetric lattice, where $v_2 \neq v_3$, can no longer be characterized using an integer Zak phase. It has been shown that it supports both topologically protected and localized, but not protected, edge states [51]. Such features can also be simulated and observed in the Rydberg composite by setting $t_2 \neq t_3$.

C. Triangular lattice

These previous two examples have demonstrated that the Rydberg composite can realize topologically interesting models, exemplified by the dimer and trimer SSH chains already studied. We now show how to realize a model with richer topology and complexity. We consider again a system with a unit cell of three lattice sites, but now connect each pair of sites within the unit cell with an equal hopping amplitude u. Each triangle is coupled to its neighbor by the hopping amplitudes a (magenta), b (green), and c (cyan, dashed), as shown in Fig. 1(ci); in general these amplitudes can all differ. We realize this Hamiltonian in the Rydberg composite by keeping the same trimer structure as before, but now utilizing one of the most appealing features of the Rydberg composite: the ease with which we can introduce long-range and oscillatory interactions to the system by changing the overall size of the ring. In general, as the radius of the ring shrinks, the interactions become longer ranged [34].

For this example, we select $\nu = 60$ and $R_2 = 1.74\nu^2$, which leads to the interaction curves $V_{qq'}$ shown in Fig. 1(ciii). These curves are approximately sinusoidal with a rapidly decreasing amplitude as $|q - q'|$ increases. To see how this choice works to engineer the desired system, consider first the pink curve, which shows the hopping amplitude from site 5 to its neighbors as a continuous function of the distance D_5 away from this site. The pink markers on this curve show the hopping amplitudes connecting site 5 to the labeled site at the specified positions. The onsite energy $E_5 = V_{55}$ is not visible on this scale. The inversion symmetry of the trimer ensures that $V_{56} = V_{54}$; more distant sites (i.e., 3 and 7) are coupled weakly to this site for the chosen value of t_1. Now, to make the couplings V_{46} equal to these couplings, we take advantage of the oscillatory interaction. Looking at the black curve, which is the same as the pink curve but relative to site 6, we can read off the values of V_{46} and V_{56}, which are identical as long as the atoms in each unit cell are an arclength $2\pi R_2/45$ apart. In general, larger unit cells with n participating atoms having identical all-to-all coupling can be engineered by finding parameters such that $V(t_2) = V(2t_2) = \ldots V(nt_2)$, where t_2 is the arclength between atoms in a cell and the $n+1$th atom is placed further at a $t_1 + nt_2$. It is not clear that such an arrangement can be found for arbitrary n, but we verified that the $n = 4$ case can be designed, utilizing a smaller ring size where the interaction envelope decays less quickly.

The band spectrum for this triangle lattice system and $M = 24$ atoms, plotted with black curves as a function of t_1, is shown in Fig. 4(a). Three bands are clearly visible. The upper two repeatedly cross one another. Outside of these crossing regions, a pair of zero-energy modes is clearly present in the band gap. Between the lower two bands there are no unambiguous edge states for this small lattice, although inspection of the eigenstates for slightly larger lattice dimensions (not shown here) suggests that the states in between the two bands in the region from $0.1 < t_1 < t_2$ are indeed edge states.

To analyze this spectrum, we turn again to the bulk Hamiltonian, which is now given by

$$H_{\text{triangle}}(k) = \begin{pmatrix} 2c\cos k & u + be^{-ik} & u + ae^{-ik} \\ u + be^{ik} & 2c\cos k & u + be^{-ik} \\ u + ae^{ik} & u + be^{ik} & 2c\cos k \end{pmatrix}. \quad (7)$$

Note that the coupling c enters the bulk Hamiltonian only on the diagonal and therefore has no impact on the gap-closing conditions or the topological phase transitions. The Hamiltonian is inversion symmetric, and therefore we can characterize its topological features using, again, the Zak phase as a quantized topological invariant. In the bottom (top) panel of Fig. 4(c), we show the phase diagram of $\mathcal{Z}$ as a function of the hopping amplitudes a and b for the lower (upper) band gap. The blue (shaded) color denotes the topological phase ($\mathcal{Z} = \pi$) and white the trivial phase ($\mathcal{Z} = 0$). The gray dashed lines show the gap closing conditions, which are sufficient but not necessary for the existence of a topological phase transition. These occur when $a = b$ or $b = \pm 2u - a$. We have computed this phase diagram for all a and b values in the plotted range, but as these depend parametrically on the arclength t_1, we cannot probe this full parameter space in the Rydberg composite. The orange curve shows the path through this parameter space that we can attain by varying t_1 over the range shown in Fig. 4(a), starting at $t_1 = 0.09$ at the marker

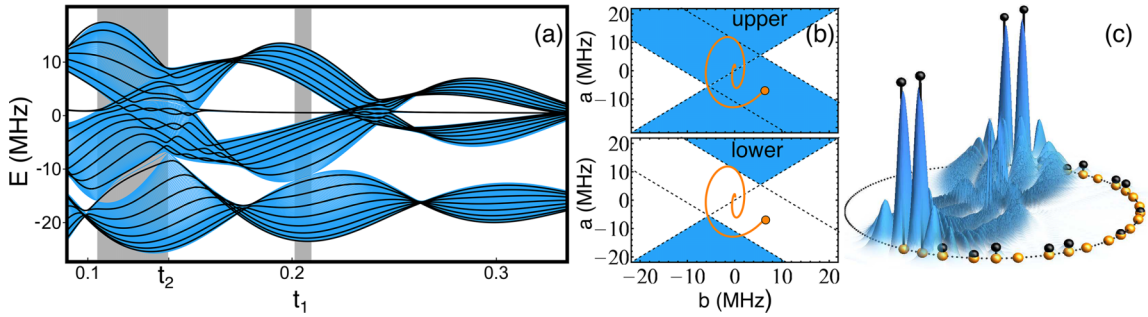

FIG. 4. (a) The energy spectrum of the triangle chain Rydberg composite. The black curves show the Rydberg energies as a function of the arclength t_1 [see Fig. 1(cii)] for $\nu = 60$, $R = 1.74\nu^2$, and $M = 24$ scatterers. The energies are centered around the onsite potential E_q, and are plotted as a function of t_1 for fixed $t_2 = 2\pi R/45$. The blue curves show the spectrum for the same lattice parameters but $M = 300$. Topologically protected edge states are found in the middle of the upper band gap for all t_1 values, although they disappear when the bands cross as discussed in the text. One of these edge states, for $t_1 = 0.2$, is shown in panel (c). The lower band gap has $\mathcal{Z} = \pi$ only within the gray shaded regions, where degenerate states in the band gap can be seen in the spectrum of the larger lattice. (b) The Zak phase of the upper and lower band gaps. Blue regions have $\mathcal{Z} = \pi$, while white regions have $\mathcal{Z} = 0$. The orange curve shows how this parameter space is traversed as we parametrically change t_1, as described in the text. Note that $u \approx -5.5$ MHz for the composite studied here.

and ending at $t_1 = 0.33$. Using this curve we can analyze the states in panel (a) with respect to their topological properties. For this choice of parameters, the orange curve in the upper band gap does not enter the region with a Zak phase of 0; for this reason there are always edge states visible when the bands are not overlapping. When the bands overlap, these edge states disappear even though the Zak phase remains equal to π. This surprising observation, contrary to the common belief that a nontrivial Zak phase implies the existence of localized edge states, has been previously observed and discussed in Refs. [56,57], but it does not seem to be widely known. In contrast, the Zak phase in the bottom gap is zero except for two intervals. These correspond to the regions highlighted in Fig. 4(a) with gray boxes. Since the spectrum in panel (a) is for only a relatively small number of scatterers, the distinction between band edges and states within the band gap is not clear. Therefore, we artificially extended the system to 300 sites and plotted the resulting spectrum in blue. The edge states in the lower band gap can now clearly be seen, at least in the larger region with $\mathcal{Z} = \pi$ just below $t_1 = t_2$. We have confirmed that these are edge states by adding disorder to the system which preserves the inversion symmetry. Under this disorder, the character of these edge states is preserved.

IV. CONCLUSION

The above examples demonstrate that with Rydberg composites one can realize Hamiltonians that exhibit a variety of interesting topological features. For the design and interpretation of the Rydberg composite we utilized the useful link between the Rydberg composite and a tight-binding Hamiltonian, which was previously elucidated in the context of Anderson localization [34]. While we did not consider disorder in the present work, defects in the positions of the ground state atoms would result in disorder in the hopping terms and onsite energies of the different models studied here, and —as long as disorder which breaks the chiral or inversion symmetries of our models could be avoided —the topological protection of the edge states predicted here could be studied.

The experimental realization of a Rydberg composite will be a challenge. While it is a routine task to excite Rydberg atoms surrounding many ground-state atoms in a random gas [58,59], placing these atoms in a specific arrangement at these length scales is difficult. Programmable optical tweezers, which have become a very powerful and versatile tool recently, would struggle to reach the ∼60 nm length scales required for the ν values selected in our examples. However, there are no fundamental obstacles here and recently even sub-50 nm spacing between traps was achieved [43]. Subwavelength [44,60,61] or dark-state [62,63] lattices can also reach ∼100 nm scales, and imaging capabilities at the sub-50 nm scale have also developed recently [64,65]. Finally, these spatial constraints can be relaxed significantly by going to larger principal quantum numbers, although this is a tradeoff as higher ν will demand better stray field control and experimental resolution.

ACKNOWLEDGMENTS

M.T.E. thanks S. Zhang for pointing out Refs. [56,57]. C.W.W. acknowledges support from the Max-Planck Gesellschaft via the MPI-PKS Next Step Fellowship and is financially supported by the Deutsche Forschungsgemeinschaft (DFG, German Research Foundation)–Project No. 496502542 (WA 5170/1-1). A.E. acknowledges support from the DFG via a Heisenberg fellowship (Grant No. EI 872/10-1).

[1] J. Moore, The next generation, Nat. Phys. **5**, 378 (2009).
[2] J. E. Moore, The birth of topological insulators, Nature (London) **464**, 194 (2010).
[3] M. Z. Hasan and J. E. Moore, Three-dimensional topological insulators, Annu. Rev. Condens. Matter Phys. **2**, 55 (2011).

[4] S. Mittal, J. Fan, S. Faez, A. Migdall, J. M. Taylor, and M. Hafezi, Topologically robust transport of photons in a synthetic gauge field, Phys. Rev. Lett. **113**, 087403 (2014).

[5] M. Lohse, C. Schweizer, O. Zilberberg, M. Aidelsburger, and I. Bloch, A Thouless quantum pump with ultracold bosonic atoms in an optical superlattice, Nat. Phys. **12**, 350 (2016).

[6] S. Nakajima, T. Tomita, S. Taie, T. Ichinose, H. Ozawa, L. Wang, M. Troyer, and Y. Takahashi, Topological Thouless pumping of ultracold fermions, Nat. Phys. **12**, 296 (2016).

[7] M. Lohse, C. Schweizer, H. M. Price, O. Zilberberg, and I. Bloch, Exploring 4D quantum Hall physics with a 2D topological charge pump, Nature (London) **553**, 55 (2018).

[8] Y. E. Kraus, Y. Lahini, Z. Ringel, M. Verbin, and O. Zilberberg, Topological states and adiabatic pumping in quasicrystals, Phys. Rev. Lett. **109**, 106402 (2012).

[9] M. Verbin, O. Zilberberg, Y. Lahini, Y. E. Kraus, and Y. Silberberg, Topological pumping over a photonic Fibonacci quasicrystal, Phys. Rev. B **91**, 064201 (2015).

[10] O. Zilberberg, S. Huang, J. Guglielmon, M. Wang, K. P. Chen, Y. E. Kraus, and M. C. Rechtsman, Photonic topological boundary pumping as a probe of 4D quantum hall physics, Nature (London) **553**, 59 (2018).

[11] C. L. Kane and T. C. Lubensky, Topological boundary modes in isostatic lattices, Nat. Phys. **10**, 39 (2014).

[12] J. Paulose, B. G. Chen, and V. Vitelli, Topological modes bound to dislocations in mechanical metamaterials, Nat. Phys. **11**, 153 (2015).

[13] G. Salerno and I. Carusotto, Dynamical decoupling and dynamical isolation in temporally modulated coupled pendulums, Europhys. Lett. **106**, 24002 (2014).

[14] R. Süsstrunk and S. D. Huber, Observation of phononic helical edge states in a mechanical topological insulator, Science **349**, 47 (2015).

[15] J. Ningyuan, C. Owens, A. Sommer, D. Schuster, and J. Simon, Time- and site-resolved dynamics in a topological circuit, Phys. Rev. X **5**, 021031 (2015).

[16] V. V. Albert, L. I. Glazman, and L. Jiang, Topological properties of linear circuit lattices, Phys. Rev. Lett. **114**, 173902 (2015).

[17] A. Aspuru-Guzik and P. Walther, Photonic quantum simulators, Nat. Phys. **8**, 285 (2012).

[18] T. Kitagawa, M. A. Broome, A. Fedrizzi, M. S. Rudner, E. Berg, I. Kassal, A. Aspuru-Guzik, E. Demler, and A. G. White, Observation of topologically protected bound states in photonic quantum walks, Nat. Commun. **3**, 882 (2012).

[19] H. Zhao, P. Miao, M. H. Teimourpour, S. Malzard, R. El-Ganainy, H. Schomerus, and L. Feng, Topological hybrid silicon microlasers, Nat. Commun. **9**, 981 (2018).

[20] J. Arkinstall, M. H. Teimourpour, L. Feng, R. El-Ganainy, and H. Schomerus, Topological tight-binding models from nontrivial square roots, Phys. Rev. B **95**, 165109 (2017).

[21] Z. Zhang, M. H. Teimourpour, J. Arkinstall, M. Pan, P. Miao, H. Schomerus, R. El-Ganainy, and L. Feng, Experimental Realization of Multiple Topological Edge States in a 1D Photonic Lattice, Laser Photon. Rev. **13**, 1800202 (2019).

[22] J. Yuen-Zhou, S. K. Saikin, N. Y. Yao, and A. Aspuru-Guzik, Topologically protected excitons in porphyrin thin films, Nat. Mater. **13**, 1026 (2014).

[23] W. P. Su, J. R. Schrieffer, and A. J. Heeger, Solitons in Polyacetylene, Phys. Rev. Lett. **42**, 1698 (1979).

[24] S. de Léséleuc, V. Lienhard, P. Scholl, D. Barredo, S. Weber, N. Lang, H. P. Büchler, T. Lahaye, and A. Browaeys, Observation of a symmetry-protected topological phase of interacting bosons with Rydberg atoms, Science **365**, 775 (2019).

[25] S. K. Kanungo, J. D. Whalen, Y. Lu, M. Yuan, S. Dasgupta, F. B. Dunning, K. R. A. Hazzard, and T. C. Killian, Realizing topological edge states with Rydberg-atom synthetic dimensions, Nat. Commun. **13**, 972 (2022).

[26] T.-H. Yang, B.-Z. Wang, X.-C. Zhou, and X.-J. Liu, Quantum Hall states for Rydberg arrays with laser-assisted dipole-dipole interactions, Phys. Rev. A **106**, L021101 (2022).

[27] R. Samajdar, W. W. Ho, H. Pichler, M. D. Lukin, and S. Sachdev, Quantum phases of Rydberg atoms on a kagome lattice, Proc. Natl. Acad. Sci. USA **118**, e2015785118 (2021).

[28] K. Li, J.-H. Wang, Y.-B. Yang, and Y. Xu, Symmetry-protected topological phases in a Rydberg glass, Phys. Rev. Lett. **127**, 263004 (2021).

[29] R. Verresen and A. Vishwanath, Unifying kitaev magnets, kagomé dimer models, and ruby Rydberg spin liquids, Phys. Rev. X **12**, 041029 (2022).

[30] G. Giudici, M. D. Lukin, and H. Pichler, Dynamical preparation of quantum spin liquids in Rydberg atom arrays, Phys. Rev. Lett. **129**, 090401 (2022).

[31] R. Samajdar, D. G. Joshi, Y. Teng, and S. Sachdev, Emergent $\mathbb{Z}_2$ gauge theories and topological excitations in Rydberg atom arrays, Phys. Rev. Lett. **130**, 043601 (2023).

[32] S. Weber, R. Bai, N. Makki, J. Mögerle, T. Lahaye, A. Browaeys, M. Daghofer, N. Lang, and H. P. Büchler, Experimentally accessible scheme for a fractional Chern insulator in Rydberg atoms, PRX Quantum **3**, 030302 (2022).

[33] M. T. Eiles, J. Pérez-Ríos, F. Robicheaux, and C. H. Greene, Ultracold molecular Rydberg physics in a high density environment, J. Phys. B: At. Mol. Opt. Phys. **49**, 114005 (2016).

[34] M. T. Eiles, A. Eisfeld, and J. M. Rost, Anderson localization of a rydberg electron, Phys. Rev. Res. **5**, 033032 (2023).

[35] A. L. Hunter, M. T. Eiles, A. Eisfeld, and J. M. Rost, Rydberg Composites, Phys. Rev. X **10**, 031046 (2020).

[36] M. T. Eiles, A. L. Hunter, and J. M. Rost, Ring Rydberg composites, J. Phys. B: At. Mol. Opt. Phys. **53**, 054001 (2020).

[37] C. H. Greene, A. S. Dickinson, and H. R. Sadeghpour, Creation of polar and nonpolar ultra-long-range Rydberg molecules, Phys. Rev. Lett. **85**, 2458 (2000).

[38] M. T. Eiles, Trilobites, butterflies, and other exotic specimens of long-range Rydberg molecules, J. Phys. B: At. Mol. Opt. Phys. **52**, 113001 (2019).

[39] E. Fermi, Sopra lo Spostamento per Pressione delle Righe Elevate delle Serie Spettrali, Il Nuovo Cimento **11**, 157 (1934).

[40] A. Omont, On the theory of collisions of atoms in Rydberg states with neutral particles, J. Phys. **38**, 1343 (1977).

[41] We neglect the role of quantum defects, as we focus on the perturbation of the degenerate hydrogen-like states with angular momentum greater than three [34].

[42] F. Cooper, A. Khare, and U. Sukhatme, Supersymmetry and quantum mechanics, Phys. Rep. **251**, 267 (1995).

[43] L. Du, P. Barral, M. Cantara, J. de Hond, Y.-K. Lu, and W. Ketterle, Atomic physics on a 50 nm scale: Realization of a bilayer system of dipolar atoms, arXiv:2302.07209.

[44] R. P. Anderson, D. Trypogeorgos, A. Valdés-Curiel, Q.-Y. Liang, J. Tao, M. Zhao, T. Andrijauskas, G. Juzeliūnas, and

I. B. Spielman, Realization of a deeply subwavelength adiabatic optical lattice, Phys. Rev. Res. **2**, 013149 (2020).

[45] We plot the absolute values of the wave functions here.

[46] J. Zak, Berry's phase for energy bands in solids, Phys. Rev. Lett. **62**, 2747 (1989).

[47] R. Resta, Macroscopic polarization in crystalline dielectrics: The geometric phase approach, Rev. Mod. Phys. **66**, 899 (1994).

[48] R. Resta, Manifestations of Berry's phase in molecules and condensed matter, J. Phys.: Condens. Matter **12**, R107 (2000).

[49] We evaluate $\mathcal{Z}$ on a discrete mesh of k points using

$$\mathcal{Z} = -\mathrm{Im}\ln\Pi_k\langle\psi_k|\psi_{k+1}\rangle, \tag{8}$$

which does not require the phase of the eigenstates $|\psi_k\rangle$ to be a continuous function of k.

[50] M. J. Rice and E. J. Mele, Elementary excitations of a linearly conjugated diatomic polymer, Phys. Rev. Lett. **49**, 1455 (1982).

[51] V. M. Martinez Alvarez and M. D. Coutinho-Filho, Edge states in trimer lattices, Phys. Rev. A **99**, 013833 (2019).

[52] A. Anastasiadis, G. Styliaris, R. Chaunsali, G. Theocharis, and F. K. Diakonos, Bulk-edge correspondence in the trimer Su-Schrieffer-Heeger model, Phys. Rev. B **106**, 085109 (2022).

[53] Z. Guo, X. Wu, S. Ke, L. Dong, F. Deng, H. Jiang, and H. Chen, Rotation controlled topological edge states in a trimer chain composed of meta-atoms, New J. Phys. **24**, 063001 (2022).

[54] J. W. Park, E. Do, J. S. Shin, S. K. Song, O. Stetsovych, P. Jelinek, and H. W. Yeom, Creation and annihilation of mobile fractional solitons in atomic chains, Nat. Nanotechnol. **17**, 244 (2022).

[55] Y. V. Kartashov, A. A. Arkhipova, S. A. Zhuravitskii, N. N. Skryabin, I. V. Dyakonov, A. A. Kalinkin, S. P. Kulik, V. O. Kompanets, S. V. Chekalin, L. Torner, and V. N. Zadkov, Observation of edge solitons in topological trimer arrays, Phys. Rev. Lett. **128**, 093901 (2022).

[56] M. Malki and G. S. Uhrig, Delocalization of edge states in topological phases, Europhys. Lett. **127**, 27001 (2019).

[57] M. Malki, L. Müller, and G. S. Uhrig, Absence of localized edge modes in spite of a non-trivial Zak phase in $BiCu_2PO_6$, Phys. Rev. Res. **1**, 033197 (2019).

[58] F. Camargo, R. Schmidt, J. D. Whalen, R. Ding, G. Woehl Jr, S. Yoshida, J. Burgdörfer, F. B. Dunning, H. R. Sadeghpour, E. Demler, and T. C. Killian, Creation of rydberg polarons in a bose gas, Phys. Rev. Lett. **120**, 083401 (2018).

[59] A. Gaj, A. T. Krupp, J. B. Balewski, R. Löw, S. Hofferberth, and T. Pfau, From molecular spectra to a density shift in dense rydberg gases, Nat. Commun. **5**, 4546 (2014).

[60] T. C. Tsui, Y. Wang, S. Subhankar, J. V. Porto, and S. L. Rolston, Realization of a stroboscopic optical lattice for cold atoms with subwavelength spacing, Phys. Rev. A **101**, 041603(R) (2020).

[61] S. Nascimbene, N. Goldman, N. R. Cooper, and J. Dalibard, Dynamic optical lattices of subwavelength spacing for ultracold atoms, Phys. Rev. Lett. **115**, 140401 (2015).

[62] M. Łącki, M. A. Baranov, H. Pichler, and P Zoller, Nanoscale "dark state" optical potentials for cold atoms, Phys. Rev. Lett. **117**, 233001 (2016).

[63] Y. Wang, S. Subhankar, P. Bienias, M. Łącki, T.-C. Tsui, M. A. Baranov, A. V. Gorshkov, P. Zoller, J. V. Porto, S. L. Rolston *et al.*, Dark state optical lattice with a subwavelength spatial structure, Phys. Rev. Lett. **120**, 083601 (2018).

[64] S. Subhankar, Y. Wang, T.-C. Tsui, S. Rolston, and J. V. Porto, Nanoscale atomic density microscopy, Phys. Rev. X **9**, 021002 (2019).

[65] M. McDonald, J. Trisnadi, K.-X. Yao, and C. Chin, Superresolution microscopy of cold atoms in an optical lattice, Phys. Rev. X **9**, 021001 (2019).